I&EC research
Industrial & Engineering Chemistry Research

Article

pubs.acs.org/IECR

# Diverse Physical States of Amorphous Precursors in Zeolite Sol Gel Syntheses

Rui Li,[†,#] Aseem Chawla,[†,#] Noemi Linares,[‡] James G. Sutjianto,[†] Karena W. Chapman,[§] Javier García Martínez,[‡] and Jeffrey D. Rimer*[,†]

[†]Department of Chemical and Biomolecular Engineering, University of Houston, Houston, Texas 77204, United States
[‡]Molecular Nanotechnology Lab, Department of Inorganic Chemistry, University of Alicante, 03690 Alicante, Spain
[§]X-ray Science Division, Advanced Photon Source, Argonne National Laboratory, Lemont, Illinois 60439, United States

Supporting Information

**ABSTRACT:** The assembly and structural evolution of amorphous precursors during zeolite crystallization is an important area of interest owing to their putative roles in the nucleation and growth of aluminosilicate microporous materials. Precursors range in complexity from oligomeric molecules and colloidal particles to gels comprised of heterogeneous silica and alumina domains. The physical state of precursors in most zeolite syntheses is generally not well understood; however, it is evident that the physicochemical properties of precursors depend on a wide range of conditions that include (but are not limited to) the selection of reagents, the composition of growth mixtures, the methods of preparation, and the use of inorganic and/or organic structure-directing agents. The fact that precursors evolve in size, shape, and/or microstructure during the course of nucleation and potentially throughout crystallization leads to questions pertaining to their mode of action in the formation of zeolites. This also highlights the diversity of species that are present in growth media, thus rendering the topic of zeolite synthesis essentially a black box to those attempting to better understand the fundamental role(s) of precursors. In this Article, we discuss the wide variety of precursors encountered in the synthesis of various framework types, emphasizing their complex physical states and the thermodynamic and kinetic factors that govern their heterogeneity.

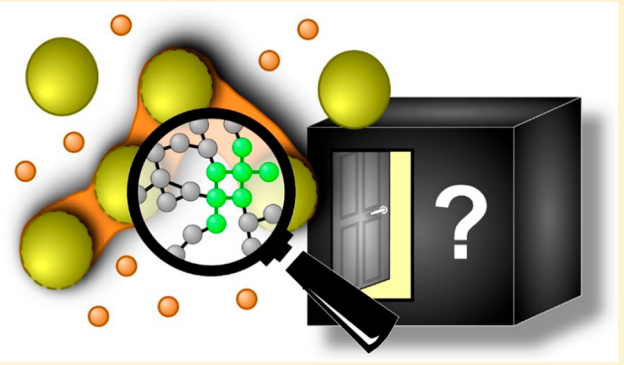


Elucidating the mechanisms of zeolite crystallization is complex owing in large part to the vast number of species present in synthesis mixtures.[1,2] This is a contributing factor to the challenges associated with zeolite crystal engineering where it is difficult to design materials with predetermined physicochemical properties without sufficient knowledge of how synthesis variables can be tailored to mediate crystal growth.[3] The ubiquitous presence of amorphous precursors throughout nucleation and growth make zeolites quintessential examples of materials that grow via *nonclassical* pathways, which include crystallization by particle attachment.[4−7] This rapidly emerging area is garnering considerable attention owing to the expanding list of materials that show evidence of growth via multifaceted pathways.[8−13] Knowledge of nonclassical mechanisms, however, is rather limited due to inadequate analytical techniques available to observe dynamic processes of growth *in situ* with sufficient spatiotemporal resolution.

In this perspective Article, we highlight the various routes leading to the assembly and evolution of amorphous precursors in zeolite synthesis wherein it is recognized that changes in conditions, most notably the selection of silica/alumina sources and room temperature aging protocols, can significantly influence polymorphism, crystallization kinetics, and the properties of zeolites, among other factors. Here, we address the physical state of precursors with an emphasis on the appropriate use of the word "gel" to properly convey the heterogeneity of these species. In most zeolite syntheses, precursors undergo structural and/or compositional changes during the induction period. The exact microstructure of the evolved precursors is not well understood, nor are the detailed processes leading to their aggregation and densification. The direct role of precursors in the mechanism of crystal growth has been suggested for several framework types, such as LTA (zeolite A),[14] FAU (zeolite X/Y),[15,16] MFI (ZSM-5),[17,18] ANA (analcime),[19] SOD (sodalite),[20] CHA (SSZ-13),[5] and EMT.[21] Characterizing the role of precursors in zeolite crystallization is an active area of research, but there is still a significant knowledge gap in the understanding of molecular-level processes governing disorder-to-order transformations in zeolite synthesis. The presence of an amorphous phase can significantly modify zeolite crystallization, for example, by lowering the energetic barrier for heterogeneous nucleation by creating

**Received:** April 18, 2018
**Revised:** May 27, 2018
**Accepted:** June 1, 2018




DOI: 10.1021/acs.iecr.8b01695
*Ind. Eng. Chem. Res.* XXXX, XXX, XXX−XXX

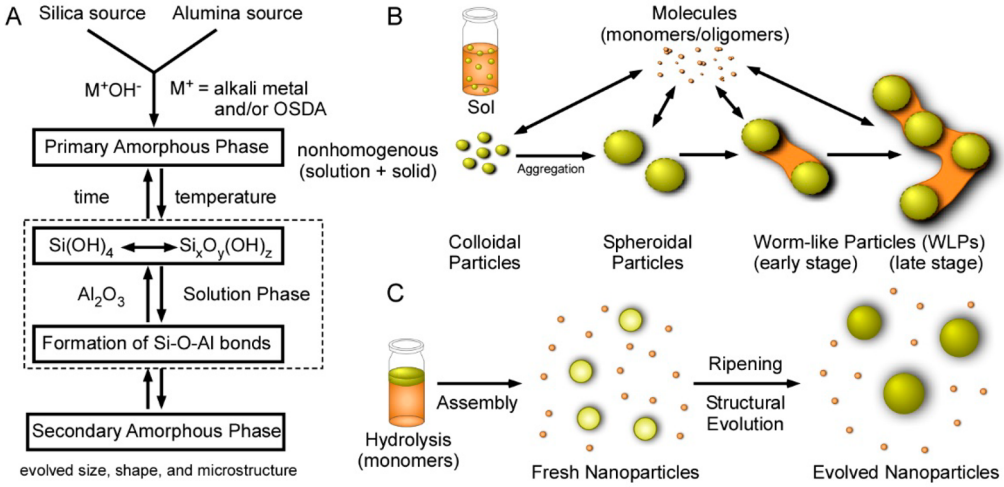


**Figure 1.** (A) General pathways leading to the formation of primary and secondary amorphous phases in zeolite synthesis. The evolving mixture is divided into the solid and solution state (the latter is illustrated in the dashed box). This scheme was adapted with permission from Cundy and Cox.[25] Copyright 2005 Elsevier Inc. (B) Schematic showing the formation of amorphous precursors in zeolite L synthesis beginning from a colloidal silica sol. Worm-like particles (WLPs) form through a series of putative aggregation, densification (or ripening), and growth processes. This scheme was adapted from Kumar et al.[26] Copyright 2016 American Chemical Society. (C) Illustration of silicalite-1 precursor assembly and evolution via TEOS hydrolysis, condensation, and Ostwald ripening.

regions of high supersaturation, analogous to the two-step nucleation mechanism postulated for other materials such as proteins, polymers, colloids, and biominerals.[12,22−24] In this Article, we do not attempt to reconcile this gap but merely seek to highlight the heterogeneous physical state that constitutes the majority of amorphous precursors observed during the preparation of (alumino)silicate zeolites.

Figure 1 depicts various processes associated with precursor formation and evolution. Figure 1A is adapted from the review of Cundy and Cox[25] showing that the initial mixing of silica and alumina in alkaline media lead to the formation of nonhomogeneous amorphous precursors comprised of undissolved sources and species exchanged between solids and solution. The dashed boxes indicate aluminosilicate speciation in the solution state where prolonged time and/or higher temperature lead to precursor evolution in size, shape, and oftentimes microstructure. The terms primary and secondary have been used to differentiate the initial self-assembled precursors from those that have evolved through either room temperature aging or hydrothermal treatment. In literature, discussions of precursor assembly and evolution often invoke simplified schematics in a manner where precursors can be misconstrued as being homogeneous. The steady state distribution of species between solid and solution is established by the degree of silica dissolution. When silica sources such as colloidal silica, fumed silica, and alkali silicate are introduced into a high pH medium in either the presence or absence of an aluminum source, they are particulates. An example of precursor evolution is illustrated in Figure 1B for zeolite L prepared with colloidal silica. The sequence of steps during hydrothermal treatment begins with the aggregation and densification of silica particles. This is followed by the "fusing" of spherical aggregates into worm-like particles (WLPs) where undissolved silica is infused within a matrix of (alumino)silicate species.[26] The exact microstructure of these evolved (or secondary) precursors is unknown; however, it has been observed by multiple groups that secondary precursors can contain localized order that differs from the primary amorphous precursors, yet the evolved particles lack long-range (periodic) order that renders them amorphous by X-ray diffraction.[27,28] For instance, evolved precursors and their corresponding solutions may contain secondary building units of the zeolite, analogous to proposed pathways of nucleation during interzeolite transformations.[29]

It is suggested in literature that silicon sources dissolve at high pH to produce a suspension of soluble monomer or oligomeric species. Once dissolved, it is posited that these species can form gels that are often initiated by first preparing separate silica and alumina mixtures at high pH and then combining them after a fixed period of aging or hydrothermal treatment. Herein, we argue that a majority of zeolite synthesis mixtures are prepared in such a manner that will never lead to the formation of gels owing to the inability to completely dissolve the silicon source. The sol gel process used to prepare zeolites involves different physical states in the synthesis medium (as depicted in Figure 2).[30−32] The mixing of reagents in zeolite synthesis can result in the formation of a *sol*, which is comprised of a suspension of colloidal particles in a continuous liquid medium. The viscosity of the suspension can vary with respect to particle volume fraction, but ultimately, the rheological properties of sols are similar to a liquid. The second state is a *colloidal (or wet) gel*, which is a dilute cross-linked network of interacting colloidal particles that are generated from the sol. The nature of this gel may also derive from polymeric chains of aluminosilicates that form a dilute cross-linked network that is predominantly comprised of liquid. The rheological properties of these gels are more similar to a solid. A fourth state would be a hybrid of polymeric and colloidal gels (not depicted in Figure 2).

The idealized drawings in Figure 2 illustrate the potential physical states of zeolite sol gel synthesis mixtures, beginning with the introduction of the silicon source that leads to a sol (Figure 2A). Either the latter can form a colloidal (or wet) gel (Figure 2B) or the silicate particles can fully dissolve to generate a *solution* (Figure 2C) of dispersed monomer and/or oligomers. While it is less common to encounter the terms "colloidal" or "wet" gels in zeolite literature, these expressions are frequently used in sol gel literature to describe the gelation of sols.[30,33,34] Here, we distinguish this phase from the view of gels in the polymer and soft matter communities where the gel state is a network of polymeric chains formed by either physical


DOI: 10.1021/acs.iecr.8b01695
Ind. Eng. Chem. Res. XXXX, XXX, XXX−XXX

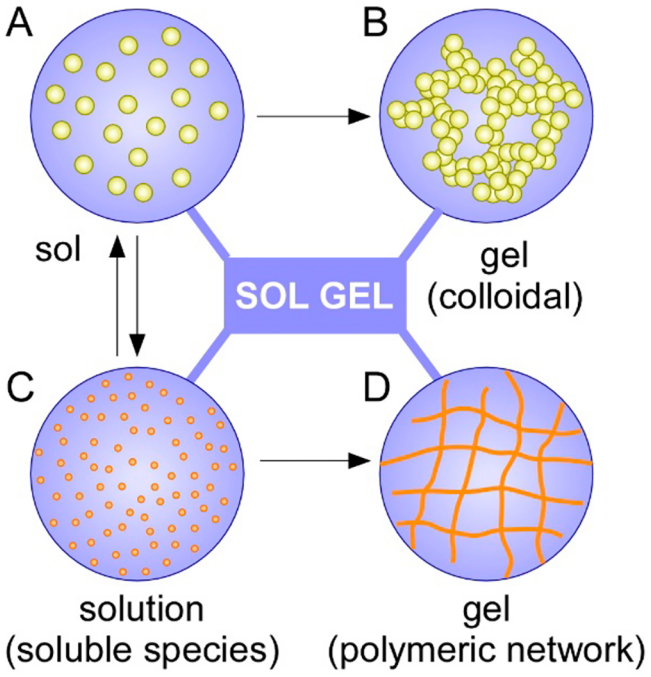


**Figure 2.** Schematic illustrating the physical states of dispersed phases of colloidal particles (yellow) and soluble species (orange) in a dispersion medium of water (blue). The four corresponding states are (A) sol, (B) colloidal (or wet) gel, (C) solution (i.e., soluble monomer and/or oligomers), and (D) gel comprised of a polymeric network of aluminosilicates. References to zeolite synthesis as a *sol gel* process implies the presence of colloids and/or polymeric aluminosilicate species (i.e., combinations of B and D). A schematic of the latter is intentionally omitted due to a lack of information regarding the microstructure of these complex phases.

aggregation or covalent bonds[35,36](represented as interconnected orange lines in Figure 2D). In the context of zeolite growth mixtures, these are tetrahedral $TO_4$ networks (T = Si or Al) derived from the condensation of soluble species. One uncertainty associated with (alumino)silicate gels is the nature of the cross-linked network. For instance, it is uncertain if the gel is comprised of covalently linked "polymer-like" chains of silicates (i.e., a chemical gel) or whether it is a network of interacting silicate species (i.e., a physical gel). We posit that the vast majority of zeolite precursor gels reported in literature are some combination of Figure 2B,D where undissolved sols are contained within a network of condensed soluble species. This is analogous to the idealized depiction of WLPs in Figure 1B where the fusing of spheroidal aggregates occurs by an exchange with soluble species, leading to interstitial regions of unknown microstructure that may be similar to a gel-like network.

The use of tetraethylorthosilicate (TEOS) as a silica source can lead to unique pathways in the formation of amorphous precursors. While TEOS is not used in the commercial production of zeolites, it is heavily utilized in academic studies to assess the mechanisms of zeolite nucleation and crystal growth.[37−44] As illustrated in Figure 1C, TEOS forms an immiscible layer above water that leads to the progressive release of soluble silicates. For detailed speciation models of TEOS hydrolysis and silica condensation, we refer readers to several prior studies.[31,32,45−47] In alkaline solvent, silicates dissociate via a series of reactions, as demonstrated here for silicic acid.[48]

$$SiO_{i-1}(OH)_{5-i}^{(i-1)-} \overset{K_m^i}{\longleftrightarrow} SiO_i(OH)_{4-i}^{i-} + H^+ \quad (1)$$

Monomers can form oligomers, and at sufficiently high TEOS concentration, these soluble silicates can further condense into nanoparticles (Figure 3A). The rate of silica condensation is

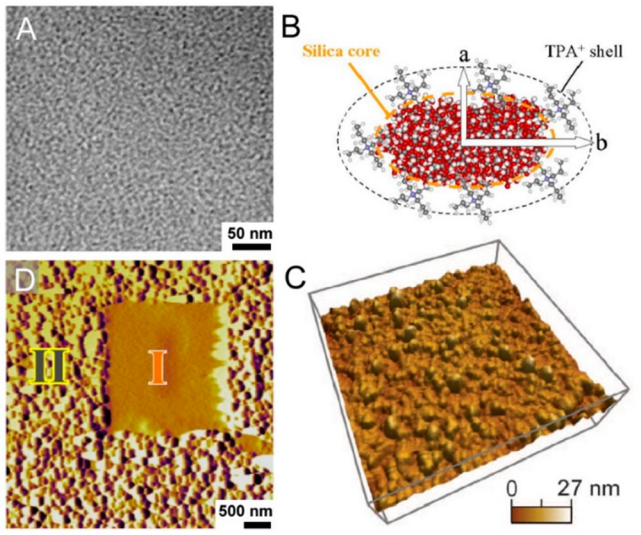


**Figure 3.** (A) Cryogenic transmission electron microscopy (cryo-TEM) image of silica nanoparticle precursors in silicalite-1 (MFI) synthesis. (Image was reprinted from ref 41. Copyright 2007 American Chemical Society.) (B) Idealized coreshell structure of nanoparticles from Monte Carlo simulations showing a shell of organic structure-directing agent (tetrapropylammonium, $TPA^+$) and a core of hydrated silica (image was provided by J.M. Fedeyko[50]). (C) Atomic force microscopy (AFM) image of a silicalite-1 surface imaged during growth in a purely siliceous solution with silica concentration of 281 mM (48 $SiO_2$/9500 $H_2O$, pH 11.2). (Image was reprinted with permission from ref 2. Copyright 2014 American Association for the Advancement of Science.) (D) AFM image of a zeolite A (LTA) surface after continuous imaging where region I is the original area of imaging and region II is a freshly imaged area after enlarging the scan area. Growth solutions are comprised of high aluminum content and a silica concentration of 10 mM. (Image was reprinted with permission from ref 51. Copyright 2018 Macmillan Publishers Limited, part of Springer Nature.)

governed by the concentration of fully protonated silicates.[49] When the nanoparticles are formed, silanol groups on their exterior surfaces as well as undercoordinated (i.e., $Q^2$ or $Q^3$) sites within the interior of the nanoparticles can undergo protonation/deprotonation depending on the pH (eq 2).

$$\equiv SiOH_{(aq)} \leftrightarrow \equiv SiO^-_{(aq)} + H^+_{(aq)} \quad (2)$$

The acid/base reactions associated with sol gel syntheses can lead to changes in pH and ionic conductivity, which reflects the chemistry of precursor assembly and evolution.

The putative structure of silica nanoparticles shown in Figure 3B was derived from Monte Carlo simulations guided by $^{29}Si$ NMR measurements of Si−O−Si connectivity.[50] The organic structure-directing agent (OSDA) tetrapropylammonium ($TPA^+$) forms a shell surrounding a core of hydrated amorphous silica.[43,52] The exact microstructure of silicalite-1 precursors is not well understood, although it is known that they evolve during the induction period. Notably, the particles grow in size by Ostwald ripening (Figure 1C)[42,49,53] and also undergo a change in structure. Analogous to secondary precursors, the microstructure of evolved nanoparticles differs from their primary state, yet they are not crystalline.[54] Nanoparticle growth ceases prior to the end of the induction period, after which the


DOI: 10.1021/acs.iecr.8b01695
Ind. Eng. Chem. Res. XXXX, XXX, XXX−XXX

precursors remain in solution throughout crystallization and there is a temporal decrease in their population during silicalite-1 formation. *In situ* atomic force microscopy (AFM) measurements of silicalite-1 (010) surface growth revealed that evolved particles attach to the crystal surface and undergo a disorder-to-order transition.[2]

Amorphous precursors generated from TEOS occur by the assembly of monomer/oligomers, whereas alternative silica sources introduced into the synthesis mixture as sols (Figure 1B) evolve into larger amorphous spheroidal particles or branched WLPs. Recent studies in our group focusing on the supernatant of sols revealed that gel-like features appear on zeolite surfaces at elevated temperature. For example, Figure 3D shows the result of an *in situ* AFM measurement of zeolite A (LTA) growth from its supernatant containing soluble aluminosilicate species where a continuously imaged area (region I) is smooth compared to the surrounding rough areas (region II). Time-resolved images of rough surface features reveal a progressive reduction in height that suggests the roughness is due to gel-like islands that form on crystal surfaces.[51] This conclusion not only was drawn from the observation that the movement of the AFM tip progressively removes material from the surface during continuous imaging but also was corroborated by chemical force microscopy measurements on the roughened gel-like regions that yielded approach−retraction profiles characteristic of elastic materials (e.g., lipid layers).

Silicon sources other than TEOS can lead to the formation of amorphous colloidal precursors that are much larger than those formed in silicalite-1 synthesis. Examples are provided in Figure 4 for two different zeolite types prepared with separate silicon sources (colloidal silica and fumed silica). Images of the precursors formed in growth mixtures of zeolite L (Figure 4A,B) are similar to those formed in the early stages of ZSM-5 growth (Figure 4C,D). The ubiquitous presence of bulk amorphous particles in zeolite growth mixtures has been widely reported for a range of frameworks including GIS, TON, MFI, CHA, and LTL. Despite their ubiquity, the role of amorphous precursors in zeolite crystallization is not fully understood. Two divergent hypotheses exist in the literature regarding the role of WLPs in zeolite nucleation (refer to Figure 9): Either WLPs can dissolve to generate molecular species that serve as growth units for crystallization or they can directly contribute to zeolite growth via pathways involving crystallization by particle attachment (or CPA).[55,56]

WLPs tend to have much higher silicon content compared to the crystalline product,[18,26] which suggests a solution-mediated process must occur during zeolite crystallization that involves the exchange of alumina from solution and significant bond breakage of Si−O−Si bonds within the WLP. The nonhomogeneous segments containing pure silica calls into question putative solid-state rearrangement of precursors to crystals. It is also uncertain to what degree precursors become locally ordered during their evolution from primary to secondary species. Analogous to schemes for zeolite L and silicate-1 (Figure 1B,C, respectively), the temporal evolution of WLPs has been observed in numerous other systems.[5,18,26,57] To illustrate the variety of pathways leading to WLP formation and evolution, we selected four different zeolite framework types and performed time-resolved analysis of precursor assembly. The structure of each zeolite selected for this study is shown in Figure 5A along with a scanning electron microscopy (SEM) image of the crystalline product. The framework types differ with respect to their composition (Si/Al ratio), the pore dimensions, and pore sizes,

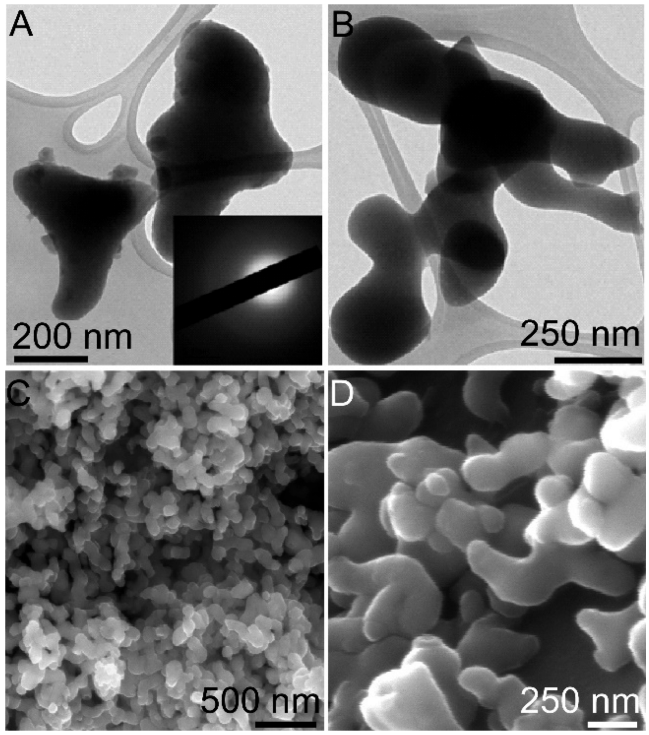


**Figure 4.** Transmission (top) and scanning (bottom) electron micrographs of amorphous precursors in zeolite growth mixtures for zeolite L (A and B) and ZSM-5 (C and D). (A) Solids extracted from a zeolite L synthesis with composition 0.5 $Al_2O_3$/20 $SiO_2$/10.2 $K_2O$/1030 $H_2O$ heated for 4 h using LUDOX AS-40 (colloidal silica) as the silicon source. (B) A similar zeolite L synthesis composition prepared with fumed silica. (C) Solids extracted from a ZSM-5 synthesis with composition 2 TPABr/11.9 $K_2O$/$Al_2O_3$/90 $SiO_2$/3588 $H_2O$ heated for 24 h using colloidal silica as the silicon source. (D) Solids extracted from a ZSM-5 synthesis with composition 2 TPABr/11.9 $K_2O$/$Al_2O_3$/90 $SiO_2$/3588 $H_2O$ heated for 24 h using fumed silica as the silicon source.

which are denoted by the n-membered rings (MRs) constituting the pore aperture: zeolite L (LTL, Si/Al = 3, 12-MR 1D pores), ZSM-22 (TON, Si/Al = 35, 10-MR 1D pores), ZSM-11 (MEL, Si/Al = 36, 10-MR, 3D pores), and ZSM-5 (MFI, Si/Al = 40, 10-MR, 3D pores).

Figure 5B plots the temporal change in precursor dimension with heating time during the synthesis of zeolite L using three different silicon sources (8 nm colloidal silica, 25 nm colloidal silica, and fumed silica). The general profile of each synthesis is a monotonic increase in precursor size (presumably through the incorporation of soluble species), followed by a plateau that coincides with the end of the induction period. The precursor size remains constant throughout zeolite L crystallization, while the population of WLPs decreases at the expense of growing crystals. For zeolite L, the silicon source has a significant impact on the induction time[26] but does not appreciably influence the rate of WLP growth. Moreover, we observe for the smallest colloidal silica (ca. 8 nm) that, once nucleation occurs, the crystallization time frame is too fast to detect WLPs (i.e., they are rapidly consumed beyond 4 h). Similar studies of other zeolites are shown in Figure 5C where we observe different trends depending on the synthesis conditions. Samples were prepared from multiple silicon sources in the presence of different OSDAs. Profiles exhibit either increasing or decreasing size with heating time, while some show relatively no change over the time period


DOI: 10.1021/acs.iecr.8b01695
*Ind. Eng. Chem. Res.* XXXX, XXX, XXX−XXX

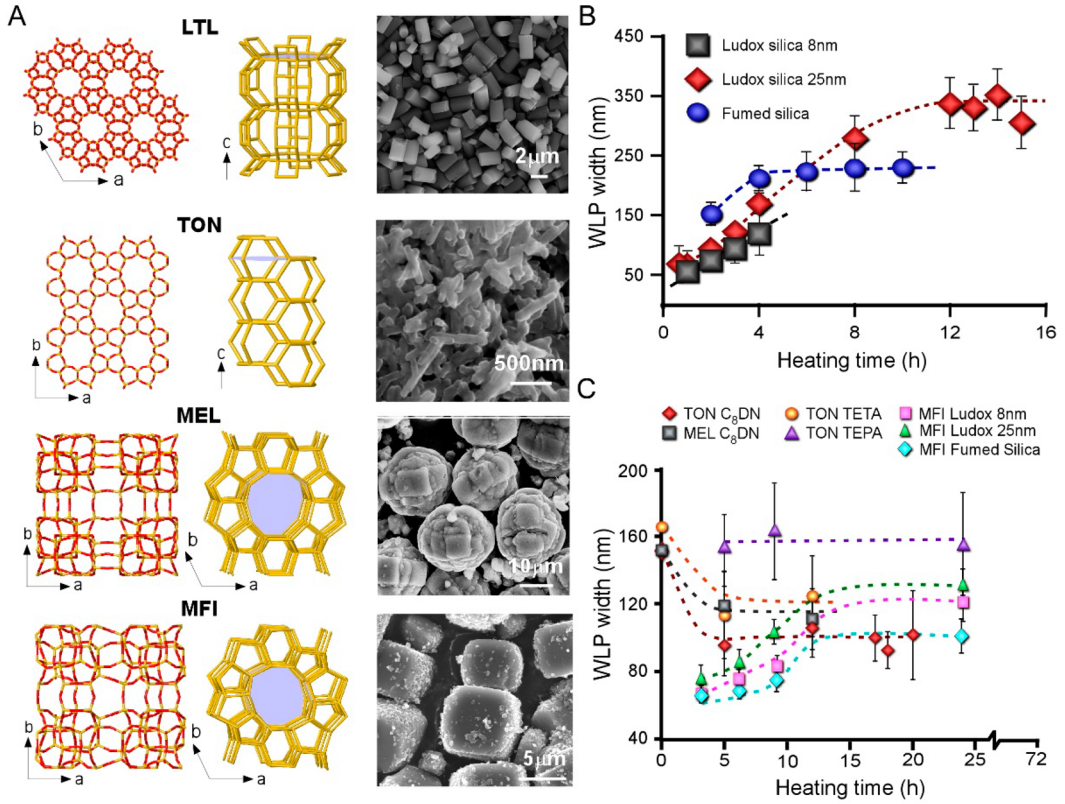


**Figure 5.** (A) Here, we select four different frameworks of varying pore size, pore dimensions, and Si/Al ratio. On the right are representative SEM images of crystals after hydrothermal treatment. (B) Temporal evolution of WLPs in K-LTL growth mixtures (OSDA-free) during hydrothermal treatment at 180 °C. Here, we plot the width of WLPs obtained from SEM images. (C) Time-resolved changes in precursor size during the synthesis of MFI, MEL, and TON syntheses at 160 °C. A variety of OSDAs were used along with different silicon sources (the OSDAs are listed in the legend, with the exception of MFI that was prepared with tetrapropylammonium). Details of each growth solution are provided in Table S1. The symbols in each plot are the average of more than 50 crystals, and error bars equal two standard deviations.

analyzed. For studies of ZSM-22, the OSDA selection effects precursor evolution. For instance, precursor size decreases in mixtures prepared with 1,8-diaminooctane ($C_8$DN) and triethylenetetramine (TETA), whereas the same composition prepared with tetraethylenepentamine (TEPA) resulted in relatively little change in precursor size. Comparisons of ZSM-5 (MFI) precursors prepared with TPA using three different silicon sources revealed analogous trends to zeolite L samples with less noticeable differences in precursor evolution. One potential cause of the disparity among samples is that the presence of OSDAs can assist in producing soluble silicates. For instance, prior studies have shown that an increased concentration of OSDA leads to an increase in pH, which impacts silica dissolution.[58,59] Given that many OSDAs exhibit positive charge (e.g., quaternary amines), it was suggested by Lowe[59] that cationic OSDAs balance the negative charge(s) of silicate anions, thereby shifting the equilibrium of silicate speciation. Iler and others have posited similar effects by showing that organic molecules such as amines and catechol can form soluble complexes with silicates, which can further accelerate silica dissolution.[31,58] Conversely, Caratzoulas and co-workers have postulated an opposite role of OSDAs to stabilize silicates by shielding siloxanes from water, thereby reducing the rate of hydrolysis (i.e., as reported for tetramethylammonium stabilization of silica cubic octamers).[60]

During the transition from primary to secondary precursors (Figure 1A), hydrothermal treatment leads to the opening of Si−O−Si bonds, whereas the presence of Si−O−Al bonds can significantly slow bond breakage at high pH. Evidence gathered from the elemental analysis of precursors in ZSM-5 and zeolite L synthesis[18,26] indicate that the silicon content can be much higher in secondary precursors than the crystalline product, which seems to indicate that the initial silicon source remains partially undissolved during the early stages of zeolite crystallization. Introduction of alumina into the growth medium can promote the aggregation of silica sols (i.e., destabilize colloidal suspensions), leading to the formation of spherical particulates that seemingly assemble via a combination of aggregation, densification (ripening), and growth processes. This general picture of precursor formation is highly suggestive that their composition is likely a hybrid of the colloidal and polymeric gels depicted in Figure 2B,D wherein the network is comprised of undissolved silica particles linked through species from solution that "bridge" opposing particles; however, it is difficult to determine individual colloidal domains in transmission electron micrographs of precursors.

One of the critical questions regarding WLP assembly pertains to the microstructure of the amorphous particles as they evolve. This alludes to more ubiquitous uncertainties regarding how we define amorphous materials. Is it sufficient to simply label systems as being either crystalline or amorphous without considering the degree of local order that has been reported in many examples of secondary (evolved) precursors? Here, we do not attempt to answer this question but merely point out that the starting materials used in the preparation of zeolite precursors can be quite different and that the evolution from


DOI: 10.1021/acs.iecr.8b01695
Ind. Eng. Chem. Res. XXXX, XXX, XXX−XXX

amorphous to crystalline is not abrupt but progressive and, moreover, that the amorphous and crystalline phases can coexist at any given time. Indeed, it is common knowledge that subtle changes in zeolite growth conditions,[61] such as the selection of silicon source, can have a pronounced impact on the final product. In some instances, zeolite syntheses will only work with a particular source, whereas other syntheses are much more robust to changes in the synthesis protocol. To ascertain the differences in Si−O−Si connectivity among three common silicon sources, we conducted pair distribution function (PDF) analysis of as received colloidal silica, fumed silica, and potassium silicate sources (Figure 6). The PDFs provide a

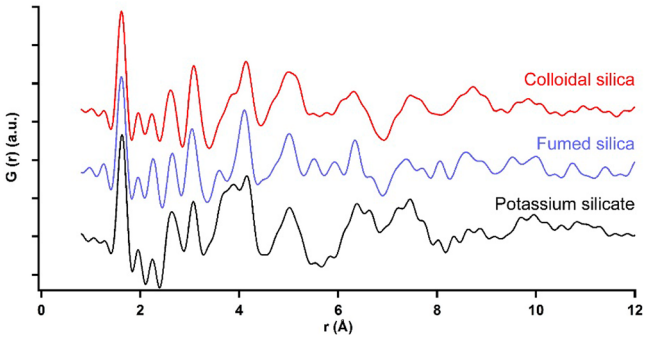


**Figure 6.** Pair distribution function (PDF) data of three common silicon sources: LUDOX AS-40 colloidal silica (red line), CAB-O-SIL fumed silica (blue line), and potassium silicate (black line). The data have been weighted ($G'(r) = G(r) \times 1.01r$) to enhance the structural differences in longer distance $r$.

histogram of all atom−atom distances within the silicate source, weighed by relative abundance and the scattering factor of the atoms. The first three peaks on all PDFs at 1.61, ∼2.6, and ∼3.1 Å correspond to the closest Si−O, O···O, and Si···Si distances, respectively, that define corner-shared $SiO_4$ tetrahedra. The potassium silicate PDF includes additional features associated with interactions (e.g., at ∼2.8 and 3.6 Å) with the $K^+$ ion. As is consistent with the noncrystalline nature of the silica sources, well-defined peaks are not observed in the PDFs at long distances, beyond ∼20 Å.

While the local tetrahedral $SiO_4$ structure and absence of long-range order is common to all silica sources in Figure 6, there are striking differences in the intermediate scale ordering from 3.5 to 12 Å. Most notably, in the PDF of fumed silica, well-defined peaks are evident at distances up to ∼12 Å, reflecting a well ordered intermediate-scale structure. Attempts to model these data showed that the structure did not correspond to the structural motifs of common dense $SiO_2$ polymorphs. While both the colloidal and potassium silicate source PDFs contain only broad/diffuse features beyond 4.5 Å, these diffuse features do not overlap, suggesting that different connectivity exists in these amorphous phases (although the correlations associated with K in the potassium silicate source will also contribute owing to differences in the structure). The broad diffuse features in the colloidal silica source shows similarities to the peaks observed for fumed silica. The difference in intermediate scale atomic structure and ordering observed for the silicon sources may account for the different solubilities or rates of reaction. If we presume that less well-ordered structures will be less thermodynamically stable, then we would expect the solubility and rates of reactions to decrease in the order potassium silicate, colloidal silica, and fumed silica.

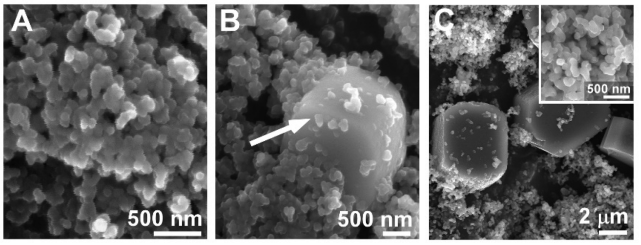


**Figure 7.** Time-resolved electron scanning micrographs of solids extracted during periodic stages of ZSM-5 synthesis. A growth mixture with molar composition 2 TPABr/11.9 $K_2O/Al_2O_3$/90 $SiO_2$/3588 $H_2O$ was heated at 160 °C. (A) Solids extracted after 3 h of heating reveal a population of amorphous WLPs. (B) Solids extracted after 6 h of heating, corresponding to the time when powder XRD patterns (Figure S1) contain the first Bragg peaks, contain larger particles (white arrow) that are most likely ZSM-5 crystals. (C) SEM images after 24 h of heating reveal a larger population of faceted ZSM-5 crystals surrounded by residual WLPs (inset). Images of samples after 48 h (not shown) reveal the disappearance of WLPs and a population of ZSM-5 crystals with an average size of 6 $\mu$m.

Figure 7A−C shows images of solids that have been extracted at periodic times during the synthesis of ZSM-5 where precursors are observed throughout crystallization. This is consistent with many zeolite syntheses where the sequence of events is similar: the precursors first assemble and evolve during the induction period; they then cease growing at a time that approximately corresponds to the onset of nucleation, and over the course of zeolite crystallization, the precursor content decreases. It is interesting that precursor assembly is rapid and that these particles exhibit a propensity to grow rather than to dissolve in highly alkaline media (i.e., pH 11−14). This prompts questions as to what degree silicon sources dissolve during room temperature aging and the early stages of hydrothermal treatment. For growth mixtures, such as those depicted in Figure 7A consisting of a high volume fraction of colloidal precursors, the samples are opaque sols or wet gels. For growth mixtures shown in Figure 3A, which consist of much smaller precursors, the samples are referred to as "clear solutions," but a more accurate description is translucent sol. It is important to note that transparent liquids do not imply the absence of colloidal particles. Indeed, the degree of opacity is dependent upon both the size and concentration of colloidal particles in the suspension. This is an important point to raise since it is often assumed that placing silica in a high pH solution will lead to complete (or nearly complete) dissolution. As we discuss herein, this does not occur for the vast majority of zeolite syntheses.

To demonstrate that silica in zeolite syntheses remain largely undissolved, we refer to a recent study[62] using dynamic light scattering (DLS) to track the temporal change in hydrodynamic diameter of colloidal silica particles in alkali hydroxide solutions (in the absence of alumina). Using a typical silica content, measurements were performed in KOH (pH 12) over a range of temperatures (25−45 °C). As shown in Figure 8A, the rate of silica dissolution increases with increased temperature, as expected. For data collected at 45 °C, we observe a plateau (dashed line in Figure 8A) once the diameter decreases by 9% of its original size. This indicates that the solution has reached thermodynamic equilibrium where an estimated 266 mM of dissolved silica corresponds to its solubility at that particular pH and temperature. During the preparation of zeolite synthesis mixtures, the addition of alumina to these colloidal suspensions leads to its deposition on the surfaces of silica particles, which


DOI: 10.1021/acs.iecr.8b01695
Ind. Eng. Chem. Res. XXXX, XXX, XXX−XXX

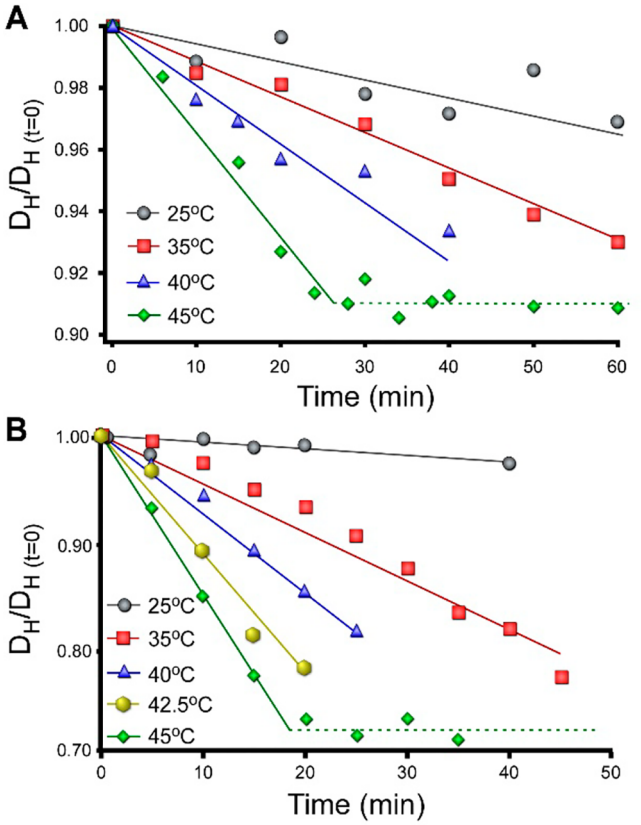


**Figure 8.** (A) Dissolution of LUDOX AS-40 colloidal silica particles in a KOH solution (pH = 12) at various temperatures (data were taken from Chawla et al.[62] with permission). The solution was prepared with 64.7 g $L^{-1}$ $SiO_2$. The change in hydrodynamic diameter $D_H$ (relative to the initial value, $D_{H(t=0)}$) was monitored by dynamic light scattering. The dashed line indicates the size reached at thermodynamic equilibrium. The colloidal particles exhibit only a 9% reduction in diameter. (B) Identical experiments in a NaOH solution (pH 13.6) prepared with 69.4 g $L^{-1}$ $SiO_2$ (data were taken from Oleksiak et al.[68] with permission). The dashed line indicates that equilibrium is reached once ca. 28% of the particle dissolves.

dramatically reduces the rate of silica dissolution. This can extend the time frame for reaching thermodynamic equilibrium or create a metastable state whereby the solution never reaches equilibrium prior to the onset of zeolite nucleation. The latter scenario was observed in a recent study where we examined silica concentrations in the supernatant of a zeolite A synthesis mixture (pH 13.7) as a function of heating time at 65 °C. In this system, silica concentrations ranged from 10 to 30 mM, which is well below the solubility of the colloidal silica used as a starting reagent.

Iler and others[63−67] have previously reported silica solubility as a function of both temperature and pH. In Table 1, we compare the solubility of amorphous silica for a limited set of conditions where it is evident that solubility increases with increasing temperature and pH. For instance, another *ex situ* DLS study at higher alkalinity using NaOH (pH 13.6) and similar silica concentration revealed that equilibrium is reached after the diameter of colloidal silica particles is reduced by ca. 28% (Figure 8B).[68] The estimated silica solubility of 725 mM at 45 °C is higher than the value in Figure 8A owing to the higher pH of the solution. Studies such as these to quantify silica solubility are limited to temperatures that are much lower than those of typical zeolites syntheses. This leads to questions regarding the actual

**Table 1. Silica Solubility for Amorphous Sources and Select Zeolites**

| material | pH | $[SiO_2]_{eq}$ (mM) | $[SiO_2]_{eq}$ (g $L^{-1}$) | references |
|---|---|---|---|---|
| amorphous silica (25 °C) | 12.0 | 318−388 | 19−23 | 63, 64 |
| LUDOX AS-40 (45 °C) | 12.0 | 266 | 16 | 62 |
| | 13.6 | 725 | 43.5 | 68 |
| zeolite LTA (25 °C) | 13.6 | 5−10 | 0.3−0.6 | 51, 72, 73 |
| zeolite MFI (25 °C) | 11.3 | 0.18 | 0.010 | this work |
| zeolite MEL (25 °C) | 11.3 | 0.21 | 0.012 | this work |
| zeolite TON (25 °C) | 11.3 | 0.21 | 0.012 | this work |

composition of solutions during the early stages of hydrothermal treatment. Notably, the ability to perform *in situ* measurements of zeolite growth solutions at high temperature to extract temporal changes in both the composition and speciation of soluble aluminosilicates could provide valuable information regarding the growth medium, particularly at critical times such as the onset of nucleation. While it is likely that such information in itself would be insufficient to elucidate the mechanism of zeolite crystallization, it could prove to be a valuable piece of the larger puzzle when trying to develop a comprehensive understanding of zeolite formation.

It has been posited that silica solubility in highly alkaline solutions (pH > 12) and at high temperature ($T$ > 100 °C) can reach values in the molar range.[64,69] Experimental validation of these predictions is challenging owing to the difficulty of *in situ* analysis. There is evidence in the literature, however, that predicted solubility may be overestimated in some instances. One example is the presence of amorphous silica nanoparticles in dilute silicalite-1 growth mixtures where *in situ* AFM measurements[2,70] of crystal surfaces (e.g., Figure 3C) reveal the presence of attached precursors at conditions that are predicted to be undersaturated. This may be due to the presence of OSDAs, which as previously mentioned, can potentially stabilize silicate species. In the context of dissolution kinetics, primary or secondary amorphous precursors may never reach thermodynamic equilibrium with soluble silicates. Moreover, measurements of silica solubility, such as that presented in Figure 8, are typically conducted in purely siliceous solutions, whereas the solubility can be quite different in actual synthesis mixtures due to the presence of alumina, metals, and organics. For example, Iler has shown that the presence of aluminum can lower silica solubility by orders of magnitude at high pH.[71] To this end, a basic understanding of the thermodynamic factors governing solution chemistry during room temperature aging and early hydrothermal treatment of zeolite synthesis mixtures is generally lacking. This presents opportunities for future studies to better understand the complex reactions of precursor assembly and evolution as well as the growth units involved in zeolite crystallization.

We measured the silica solubility for several zeolite framework types after allowing sufficient time for complete crystallization (e.g., 72 h). The corresponding solubilities listed in Table 1 were measured at 25 °C by extracting the supernatant and analyzing its Si content using inductively coupled plasma (ICP). In Table 1, we also list reported solubilities of other zeolites, such as LTA, to illustrate an upper range of silica solubility at higher pH. It is interesting to compare these values to those in Table 2 listing the silica contents used in synthesis mixtures of commonly studied zeolite framework types. The range of values listed in Table 2 are


DOI: 10.1021/acs.iecr.8b01695
Ind. Eng. Chem. Res. XXXX, XXX, XXX−XXX

**Table 2. Range of Silica Content in Zeolite Synthesis Mixtures**[a]

| zeolite | $[SiO_2]$ (g $L^{-1}$) | zeolite | $[SiO_2]$ (g $L^{-1}$) |
|---|---|---|---|
| AEI | 84−1020 | MER | 24−240 |
| BEA* | 111−477 | MFI | 2−90 |
| CHA | 72−600 | MOR | 74−420 |
| FAU | 11−167 | MTT | 56−256 |
| FER | 24−660 | MTW | 56−256 |
| GIS | 9−270 | MWW | 74−248 |
| HEU | 480−3120 | RHO | 180−540 |
| LTA | 14−96 | TON | 61−222 |
| LTL | 48−330 | UFI | 111 |
| MEL | 54−360 | | |

[a]Literature references for each framework type are provided in Table S2.

based on a limited survey of literature and, therefore, do not represent the absolute lower and upper bounds. Nevertheless, they provide an approximate range of values where it is clearly evident that the vast majority of syntheses utilize silica content well in excess of the amorphous silica solubility. Under such conditions, it is impossible to fully dissolve silica. Only under rare cases where concentrations fall below 18 g $L^{-1}$, such as purely siliceous MFI (silicalite-1) and MEL (silicalite-2), is it feasible to achieve growth solutions of dissolved silicate species. Several aluminosilicate zeolites are also prepared with low silica content (e.g., FAU, GIS, LTA, MFI); however, silica content in zeolite syntheses typically exceed 60 g $L^{-1}$. It should be noted that it is difficult to calculate and report the supersaturation with respect to silica due to the complexity of the medium given the presence of numerous species (i.e., monomers, a wide range of soluble aluminosilicate oligomers, and silica that is retained within metastable colloidal precursors). Likewise, it is challenging to isolate supernatants from zeolite growth mixtures during the hydrothermal treatment to measure their solubility at more relevant conditions. Comparisons made here are done on the basis of room temperature data listed in Table 1.

It is evident from the high silica content used in the starting mixtures of zeolite synthesis that aging silica sources in alkaline media will not result in the complete dissolution of silica particles prior to zeolite nucleation. A more realistic scenario is that the equilibrium between silica and silicate species (monomer and small oligomers) at a given pH is shifted toward the dissolution of silica as they are consumed during zeolite crystallization according to the following simplified processes:

$$\text{silica (s)} \leftrightarrow \text{silicates (aq)} \rightarrow \text{zeolite (s)} \quad (3)$$

The kinetics of silica dissolution and the evolution of its properties (e.g., porosity, microstructure, etc.) during zeolite growth are frequently overlooked and, in some cases, to the point that it is assumed silica completely dissolves during aging, which is inconsistent with the low solubility of silica relative to the high silica content of many zeolite syntheses. This is particularly relevant for synthesis protocols that separately age (or pretreat) silicon and aluminum sources prior to their mixing[74] relative to those that combine sources before aging.[68] In the former case, gelation is often observed when separately aged sources are combined; however, it should be noted that these sol gels contain undissolved silica particles. The densification process leading to what appears in electron microscopy images as a uniform spheroidal particle suggests that silica particles are interconnected through a network of condensed soluble species, which promote aggregation. The exact microstructure of amorphous precursors still remains a mystery, though it is evident that primary and secondary precursors exhibit a large degree of heterogeneity with respect to the spatial distribution of Si and Al owing, in part, to the incomplete dissolution of silicon sources. Differences in the viscosity of sol and gel mixtures can presumably influence zeolite crystallization by altering mass transport between solution and solid phases. It remains to be determined if gelation persists at higher temperature and to what degree the distribution of (alumino)silicate species between the solution and solid states varies as a function of the aging process. On the basis of the preponderance of evidence in literature that aging can significantly alter zeolite syntheses, it would come as no surprise that the selection of silicon and aluminum sources, the order of mixing these sources, and procedures for room temperature or hydrothermal treatment can impact zeolite growth and the physicochemical properties of the crystalline product.

References to amorphous precursors as *gels* coupled with the use of oversimplified schematics that depict these species as homogeneous entities can lead to misconceptions regarding their composition and structure. Cundy and Cox[25] addressed this point by stating that "the primary amorphous phase represents the initial and immediate product from the reactants and is a non-equilibrium and probably heterogeneous product containing (for example) (a) precipitated amorphous aluminosilicates, (b) coagulated silica and alumina precipitated from starting materials destabilized by the change in pH and increase in salt content and (c) unchanged reactants." In cases where synthesis protocols are designed to first dissolve silica by aging sols at high pH, this can only be accomplished at silica content below 15 g $L^{-1}$ at room temperature or around 60 g $L^{-1}$ for mixtures at higher temperature and pH. The presence of alumina, however, makes it difficult to reach saturation owing to a reduced rate of silica dissolution. It is also possible that zeolite nucleation occurs prior to reaching equilibrium between the solution and amorphous precursors ($K_2$ in Figure 9), in which case the driving force for (alumino)silicate speciation is governed by the equilibrium between the solution and crystalline phase ($K_1$ in Figure 9). This can lead to a monotonic decrease in soluble species during crystal

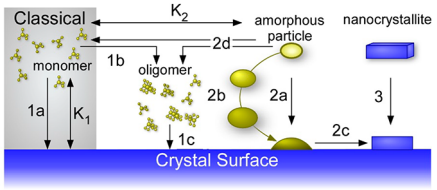


**Figure 9.** Putative pathways of zeolite crystal growth from a diverse selection of precursors. (Scheme adapted from Olafson et al.[55] Copyright 2016 American Chemical Society.) (1a) The classical pathway involves monomer-by-monomer addition (shaded gray region). The solubility constant $K_1$ signifies equilibrium between zeolite crystals and solution species at the completion of growth. Soluble species may also form oligomers (1b), which can directly attach to the crystal (1c). Soluble species can reach equilibrium $K_2$ with amorphous precursors that can add to the crystal surface (2a), evolve into secondary phases (2b) prior to their addition, or dissolve (2d) to generate soluble species. Once adsorbed to the zeolite surface, a disorder-to-order transition (2c) must occur in order for precursors to incorporate into the underlying crystal. (3) An additional pathway for zeolite crystal growth is (nearly) oriented attachment of crystallites in solution, which was recently observed for zeolite A.[51]


DOI: 10.1021/acs.iecr.8b01695
Ind. Eng. Chem. Res. XXXX, XXX, XXX−XXX

growth until the silicates concentration is on the order of 0.1−10 mM (or 0.006−6 g $L^{-1}$).

The exact role(s) of amorphous precursors in zeolite crystallization is a subject of ongoing investigation. Figure 9 depicts several pathways of zeolite growth that can be categorized as either classical (involving monomer addition) or nonclassical (involving the addition of species more complex than monomers). The mere presence of precursors implies their role in the latter pathway, although evidence shows that both classical and nonclassical pathways are involved with the former becoming more prevalent at later stages of growth when the population of precursors is small and the supersaturation of soluble silicate species is low. It is feasible that precursors serve as a reservoir of nutrient that is released by dissolution (path 2d in Figure 9), although the fact that precursor size remains constant during crystallization suggests that not all precursors dissolve, which implies that such processes are rapid and likely occur in the proximity of zeolite crystal surfaces. If precursors directly attach to crystal surfaces (eq 3; paths 2a and 2b in Figure 9), this process requires a disorder-to-order transition (path 2c in Figure 9). Indeed, there is still much that we do not know regarding the microstructure of precursors and to what degree this structure changes during primary-to-secondary phase evolution. The lack of long-range order coupled with the presence of purely siliceous regions within these phases indicates that a significant amount of bond breaking and reforming is required to transition from nonhomogeneous precursors to a final zeolite where the Si and Al are more uniformly distributed.

In this perspective Article, we reemphasize the heterogeneity of gels encountered in zeolite synthesis mixtures. In general, gels encompass a broad spectrum of physical states. Classical polymer literature defines gels as having four possible configurations: (1) well-ordered lamellar structures; (2) covalent polymeric networks, completely disordered; (3) polymer networks formed through physical aggregation, predominantly disordered; (4) particular disordered structures.[30,75] In Brinker and Scherer's book on sol gel science,[32] a signature property of the gel is defined by the combination of continuous solid and fluid phases wherein "one could travel through the solid phase from one side of the sample to the other without having to enter the liquid." These definitions allow significant latitude for the classification of gels in zeolite synthesis. Our intent is to highlight that many of the gels formed in zeolite growth mixtures are comprised of colloidal particles. To this end, any mechanism of zeolite growth involving precursors must take into account the fraction of undissolved silicon source that requires substantial bond breakage and reordering. Questions pertaining to how the physical state of the synthesis mixture (i.e., sol vs gel) impacts crystallization pathways and/or kinetics, as well as the preservation of the physical state at high temperatures relevant to the majority of zeolite syntheses, remain elusive. It is also important to better characterize, clarify, and describe the diverse family of materials that are broadly referred to as "amorphous precursors", as it is evident that a simple demarcation of crystalline versus noncrystalline is an insufficient description to explain the complex effects that source selection and aging have on zeolite synthesis.

## ■ ASSOCIATED CONTENT

### Supporting Information

The Supporting Information is available free of charge on the ACS Publications website at DOI: 10.1021/acs.iecr.8b01695.

Experimental methods; details of synthesis conditions for samples in Figure 5; powder X-ray diffraction patterns of select samples; references used to gather the information in Table 2 (PDF)

## ■ AUTHOR INFORMATION


### Corresponding Author

*E-mail jrimer@central.uh.edu.

### ORCID

Rui Li: 0000-0002-1305-2139

Karena W. Chapman: 0000-0002-8725-5633

Javier García Martínez: 0000-0002-7089-4973

Jeffrey D. Rimer: 0000-0002-2296-3428


### Author Contributions

#R.L. and A.C. contributed equally.

### Notes

The authors declare no competing financial interest.

### Biographies

**Dr. Rui Li** received dual Bachelor degrees in Chemical Engineering and Technology and English from East China University of Science and Technology in Shanghai. He received his PhD in Chemical Engineering from the University of Houston. His research focuses on the rational design of zeolites using systematic approaches with the goal of elucidating the complex mechanisms of crystal growth and tailoring material properties for various applications.

**Aseem Chawla** received his bachelor's degree in Chemical Engineering from IIT (BHU) Varanasi in India. He is now pursuing his PhD degree in Chemical Engineering under the supervision of Professor Jeffrey D. Rimer at the University of Houston. His current research is focused on elucidating the role of surfactants in zeolite catalyst synthesis and optimization.



DOI: 10.1021/acs.iecr.8b01695
Ind. Eng. Chem. Res. XXXX, XXX, XXX−XXX

**Dr. Noemi Linares** obtained her PhD Degree in 2010 at the Molecular Nanotechnology Lab in the University of Alicante (Spain), under the supervision of Prof. García Martínez. After her dissertation, she moved to Florence (Italy) for a postdoctoral fellow at the ICCOM-CNR, where she was working under the ITN NANO-HOST on the immobilization of homogeneous catalysts in nanostructured materials, mainly for the synthesis of fine-chemicals under flow conditions. In May 2013, she moved back to the University of Alicante where she is now Distinguished Research Fellow. Her research interests range from materials science to nanotechnology, heterogeneous catalysis, and flow chemistry.

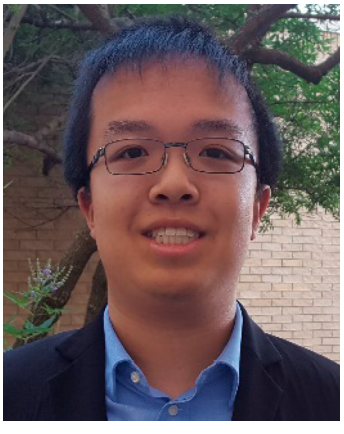

**James G. Sutjianto** received his BS degree in Chemical Engineering from The University of Houston. He is currently pursuing his PhD in Chemical Engineering at The Pennsylvania State University. His research interests are in the fields of experimental and computational materials science and catalysis/reaction engineering.

**Dr. Karena Chapman** develops and applies advanced synchrotron-based characterization tools to explore the coupling of structure and reactivity of energy-relevant materials. Specifically, her research exploits pair distribution function (PDF) analysis, often applied *in situ*, to probe the atomic and nanoscale structure of crystalline, nano, and amorphous materials that are beyond the limits of conventional crystallography. This is particularly relevant to understanding synthetic reactions, including zeolite formation, as these studies can capture the whole reaction, from the structure of amorphous precursors to the formation of the initial nuclei and how these aggregate and grow to form extended architectures. She received her B.Sc. and PhD in Chemistry from the University of Sydney, Australia, before joining Argonne National Laboratory in 2005 as the Arthur Holly Compton Postdoctoral Scholar. Following 13 years at Argonne's Advanced Photon Source, she moved to Stony Brook University in 2018 as the Joseph W Lauher and Frank W Fowler Professor of Materials Chemistry. She has been recognized as one of the American Chemical Society's Talented 12 in 2016 and was awarded the 2015 MRS Outstanding Young Investigator Award for her contributions to understanding the coupled structure and reactivity of energy-relevant systems and for developing the incisive experimental and analytical tools needed to interrogate these complex materials systems.

**Prof. Javier Garcia-Martinez** is the Director of the Molecular Nanotechnology Lab at the University of Alicante, Spain. He has published extensively in the areas of zeolites and nanotechnology and is coinventor of more than 25 patents. His latest books are "Nanotechnology for the Energy Challenge" (Wiley 2013), "Chemistry Education" (Wiley 2014), and "Mesoporous Zeolites" (Wiley 2015). He is also cofounder and Chief Scientist of Rive Technology, Inc. (Boston, USA), a venture capital-funded Massachusetts Institute of Technology (MIT) spin-off commercializing hierarchical zeolites for refining applications. He has received numerous awards including the TR35 Award from MIT's Technology Review, the Rey Jaime I Award, and the Emerging Researcher Award and the Kathryn C. Hach Award from the American Chemical Society. He is a member of the World Economic Forum, Fellow of the Royal Society of Chemistry, and member of the Executive Committee of IUPAC.

**Prof. Jeffrey D. Rimer** is the Ernest J. and Barbara M. Henley Professor of Chemical Engineering at the University of Houston. He received B.S.



DOI: 10.1021/acs.iecr.8b01695
*Ind. Eng. Chem. Res.* XXXX, XXX, XXX−XXX

degrees in Chemical Engineering and Chemistry from Washington University in St. Louis and Allegheny College, respectively. In 2006, he received his Ph.D. in Chemical Engineering from the University of Delaware. Prior to joining the Department of Chemical and Biomolecular Engineering at Houston, he spent two years as a postdoctoral fellow at New York University. He has more than 60 publications and is a coinventor on more than 12 patent applications. He has received numerous awards, including the NSF CAREER Award, the 2016 Owens Corning Early Career Award from AIChE, the 2017 FRI/John G. Kunesh Award from AIChE, and the 2018 Norman Hackerman Award in Chemical Research from the Welch Foundation. He is an executive committee member for the American Associate for Crystal Growth, vice chair of the International Zeolite Association Synthesis Commission, and chair for the GRC on Crystal Growth & Assembly and the GRC on Nanoporous Materials and Their Applications.

## ■ ACKNOWLEDGMENTS

J.D.R. acknowledges financial support from the National Science Foundation (DMREF Award 1629398), the U.S. Department of Energy, Office of Science, Office of Basic Energy Sciences under Award Number DE-SC0014468, and the Welch Foundation (Award E-1794). N.L. acknowledges support from the University of Alicante under the project GRE15-07. Work done at Argonne and use of the Advanced Photon Source, an Office of Science User Facility operated for the U.S. Department of Energy Office of Science by Argonne National Laboratory, were supported by the U.S. Department of Energy under Contract No. DE-AC02-06CH11357.

## ■ REFERENCES

(1) Grand, J.; Awala, H.; Mintova, S. Mechanism of zeolites crystal growth: new findings and open questions. *CrystEngComm* **2016**, *18* (5), 650−664.

(2) Lupulescu, A. I.; Rimer, J. D. In Situ Imaging of Silicalite-1 Surface Growth Reveals the Mechanism of Crystallization. *Science* **2014**, *344* (6185), 729.

(3) Rimer, J. D.; Chawla, A.; Le, T. T. Crystal Engineering for Catalysis. *Annu. Rev. Chem. Biomol. Eng.* **2018**, DOI: 10.1146/annurev-chembioeng-060817-083953.

(4) De Yoreo, J. J.; Gilbert, P. U. P. A.; Sommerdijk, N. A. J. M.; Penn, R.L.; Whitelam, S.; Joester, D.; Zhang, H.; Rimer, J.D.; Navrotsky, A.; Banfield, J.F.; Wallace, A.F.; Michel, F.M.; Meldrum, F.C.; Cölfen, H.; Dove, P.M. Crystallization by particle attachment in synthetic, biogenic, and geologic environments. *Science* **2015**, *349* (6247), aaa6760.

(5) Kumar, M.; Luo, H.; Román-Leshkov, Y.; Rimer, J. D. SSZ-13 Crystallization by Particle Attachment and Deterministic Pathways to Crystal Size Control. *J. Am. Chem. Soc.* **2015**, *137* (40), 13007−13017.

(6) Zhang, H.; Zhang, H.; Zhao, Y.; Shi, Z.; Zhang, Y.; Tang, Y. Seeding Bundlelike MFI Zeolite Mesocrystals: A Dynamic, Nonclassical Crystallization via Epitaxially Anisotropic Growth. *Chem. Mater.* **2017**, *29* (21), 9247−9255.

(7) Zhao, Y.; Zhang, H.; Wang, P.; Xue, F.; Ye, Z.; Zhang, Y.; Tang, Y. Tailoring the Morphology of MTW Zeolite Mesocrystals: Intertwined Classical/Nonclassical Crystallization. *Chem. Mater.* **2017**, *29* (8), 3387−3396.

(8) Zheng, H.; Smith, R. K.; Jun, Y.-w.; Kisielowski, C.; Dahmen, U.; Alivisatos, A. P. Observation of Single Colloidal Platinum Nanocrystal Growth Trajectories. *Science* **2009**, *324* (5932), 1309.

(9) Liao, H.-G.; Cui, L.; Whitelam, S.; Zheng, H. Real-Time Imaging of Pt3Fe Nanorod Growth in Solution. *Science* **2012**, *336* (6084), 1011.

(10) Habraken, W.; Tao, J.H.; Brylka, L.J.; Friedrich, H.; Bertinetti, L.; Schenk, A.S.; Verch, A.; Dmitrovic, V.; Bomans, P. H. H.; Frederik, P.M.; Laven, J.; van der Schoot, P.; Aichmayer, B.; de With, G.; DeYoreo, J.J.; Sommerdijk, N. Ion-association complexes unite classical and non-classical theories for the biomimetic nucleation of calcium phosphate. *Nat. Commun.* **2013**, *4*, 1507.

(11) Mukherjee, S.; Kim, K.; Nair, S. Short, Highly Ordered, Single-Walled Mixed-Oxide Nanotubes Assemble from Amorphous Nanoparticles. *J. Am. Chem. Soc.* **2007**, *129* (21), 6820−6826.

(12) Nielsen, M. H.; Aloni, S.; De Yoreo, J. J. In situ TEM imaging of $CaCO_3$ nucleation reveals coexistence of direct and indirect pathways. *Science* **2014**, *345* (6201), 1158.

(13) Li, D.; Nielsen, M. H.; Lee, J. R. I.; Frandsen, C.; Banfield, J. F.; De Yoreo, J. J. Direction-Specific Interactions Control Crystal Growth by Oriented Attachment. *Science* **2012**, *336* (6084), 1014.

(14) Mintova, S.; Olson, N. H.; Valtchev, V.; Bein, T. Mechanism of Zeolite A Nanocrystal Growth from Colloids at Room Temperature. *Science* **1999**, *283* (5404), 958.

(15) Valtchev, V. P.; Bozhilov, K. N. Transmission Electron Microscopy Study of the Formation of FAU-Type Zeolite at Room Temperature. *J. Phys. Chem. B* **2004**, *108* (40), 15587−15598.

(16) Valtchev, V.; Rigolet, S.; Bozhilov, K. N. Gel evolution in a FAU-type zeolite yielding system at 90°C. *Microporous Mesoporous Mater.* **2007**, *101* (1), 73−82.

(17) Chang, C. D.; Bell, A. T. Studies on the mechanism of ZSM-5 formation. *Catal. Lett.* **1991**, *8* (5), 305−316.

(18) Ren, N.; Subotić, B.; Bronić, J.; Tang, Y.; Dutour Sikirić, M.; Mišić, T.; Svetličić, V.; Bosnar, S.; Antonić Jelić, T. Unusual Pathway of Crystallization of Zeolite ZSM-5 in a Heterogeneous System: Phenomenology and Starting Considerations. *Chem. Mater.* **2012**, *24* (10), 1726−1737.

(19) Chen, X.; Qiao, M.; Xie, S.; Fan, K.; Zhou, W.; He, H. Self-Construction of Core−Shell and Hollow Zeolite Analcime Icositetrahedra: A Reversed Crystal Growth Process via Oriented Aggregation of Nanocrystallites and Recrystallization from Surface to Core. *J. Am. Chem. Soc.* **2007**, *129* (43), 13305−13312.

(20) Greer, H.; Wheatley, P. S.; Ashbrook, S. E.; Morris, R. E.; Zhou, W. Early Stage Reversed Crystal Growth of Zeolite A and Its Phase Transformation to Sodalite. *J. Am. Chem. Soc.* **2009**, *131* (49), 17986−17992.

(21) Melinte, G.; Georgieva, V.; Springuel-Huet, M. A.; Nossov, A.; Ersen, O.; Guenneau, F.; Gedeon, A.; Palčić, A.; Bozhilov Krassimir, N.; Pham-Huu, C.; Qiu, S.; Mintova, S.; Valtchev, V. 3D Study of the Morphology and Dynamics of Zeolite Nucleation. *Chem. - Eur. J.* **2015**, *21* (50), 18316−18327.

(22) Vekilov, P. G. Dense Liquid Precursor for the Nucleation of Ordered Solid Phases from Solution. *Cryst. Growth Des.* **2004**, *4* (4), 671−685.

(23) Vekilov, P. G. Two-step mechanism for the nucleation of crystals from solution. *J. Cryst. Growth* **2005**, *275* (1), 65−76.

(24) Vorontsova, M. A.; Maes, D.; Vekilov, P. G. Recent advances in the understanding of two-step nucleation of protein crystals. *Faraday Discuss.* **2015**, *179* (0), 27−40.

(25) Cundy, C. S.; Cox, P. A. The hydrothermal synthesis of zeolites: Precursors, intermediates and reaction mechanism. *Microporous Mesoporous Mater.* **2005**, *82* (1), 1−78.

(26) Kumar, M.; Li, R.; Rimer, J. D. Assembly and Evolution of Amorphous Precursors in Zeolite L Crystallization. *Chem. Mater.* **2016**, *28* (6), 1714−1727.

(27) Walton, R. I.; Millange, F.; O'Hare, D.; Davies, A. T.; Sankar, G.; Catlow, C. R. A. An in Situ Energy-Dispersive X-ray Diffraction Study of the Hydrothermal Crystallization of Zeolite A. 1. Influence of Reaction Conditions and Transformation into Sodalite. *J. Phys. Chem. B* **2001**, *105* (1), 83−90.

(28) Burkett, S. L.; Davis, M. E. Mechanism of Structure Direction in the Synthesis of Si-ZSM-5: An Investigation by Intermolecular 1H-29Si CP MAS NMR. *J. Phys. Chem.* **1994**, *98* (17), 4647−4653.

(29) Corma, A.; Li, C.; Moliner, M. Building zeolites from pre-crystallized units: nanoscale architecture. *Angew. Chem., Int. Ed.* **2018**, DOI: 10.1002/anie.201711422.

(30) Hench, L. L.; West, J. K. The sol-gel process. *Chem. Rev.* **1990**, *90* (1), 33−72.

(31) Iler, R. K. *The Chemistry of Silica: Solubility, Polymerization, Colloid and Surface Properties and Biochemistry of Silica*; Wiley: New York, 1979.

(32) Brinker, C.; Scherer, G. *Sol-Gel Science: The Physics and Chemistry of Sol-Gel Processing.*; Academic Press: New York, 1990.



DOI: 10.1021/acs.iecr.8b01695
*Ind. Eng. Chem. Res.* XXXX, XXX, XXX−XXX

(33) Feinle, A.; Elsaesser, M. S.; Husing, N. Sol-gel synthesis of monolithic materials with hierarchical porosity. *Chem. Soc. Rev.* **2016**, *45* (12), 3377−3399.
(34) Tian, T.; Zeng, Z.; Vulpe, D.; Casco, M. E.; Divitini, G.; Midgley, P. A.; Silvestre-Albero, J.; Tan, J.-C.; Moghadam, P. Z.; Fairen-Jimenez, D. A sol−gel monolithic metal−organic framework with enhanced methane uptake. *Nat. Mater.* **2017**, *17*, 174.
(35) Flory, P. J. Introductory lecture. *Faraday Discuss. Chem. Soc.* **1974**, *57* (0), 7−18.
(36) Estroff, L. A.; Hamilton, A. D. Water Gelation by Small Organic Molecules. *Chem. Rev.* **2004**, *104* (3), 1201−1218.
(37) Fan, W.; Meneau, F.; Bras, W.; Ogura, M.; Sankar, G.; Okubo, T. Effects of silicon sources on the formation of nanosized LTA: An in situ small angle X-ray scattering and wide angle X-ray scattering study. *Microporous Mesoporous Mater.* **2007**, *101* (1), 134−141.
(38) Zhu, G.; Qiu, S.; Yu, J.; Sakamoto, Y.; Xiao, F.; Xu, R.; Terasaki, O. Synthesis and Characterization of High-Quality Zeolite LTA and FAU Single Nanocrystals. *Chem. Mater.* **1998**, *10* (6), 1483−1486.
(39) Ravishankar, R.; Kirschhock, C. E. A.; Knops-Gerrits, P. P.; Feijen, E. J. P.; Grobet, P. J.; Vanoppen, P.; De Schryver, F. C.; Miehe, G.; Fuess, H.; Schoeman, B. J.; Jacobs, P. A.; Martens, J. A. Characterization of nanosized material extracted from clear suspensions for MFI zeolite synthesis. *J. Phys. Chem. B* **1999**, *103* (24), 4960−4964.
(40) Kirschhock, C. E. A.; Ravishankar, R.; Jacobs, P. A.; Martens, J. A. Aggregation mechanism of nanoslabs with zeolite MFI-type structure. *J. Phys. Chem. B* **1999**, *103* (50), 11021−11027.
(41) Kumar, S.; Davis, T. M.; Ramanan, H.; Penn, R. L.; Tsapatsis, M. Aggregative Growth of Silicalite-1. *J. Phys. Chem. B* **2007**, *111* (13), 3398−3403.
(42) Davis, T. M.; Drews, T. O.; Ramanan, H.; He, C.; Dong, J.; Schnablegger, H.; Katsoulakis, M. A.; Kokkoli, E.; McCormick, A. V.; Penn, R. L.; Tsapatsis, M. Mechanistic principles of nanoparticle evolution to zeolite crystals. *Nat. Mater.* **2006**, *5*, 400.
(43) Fedeyko, J. M.; Rimer, J. D.; Lobo, R. F.; Vlachos, D. G. Spontaneous Formation of Silica Nanoparticles in Basic Solutions of Small Tetraalkylammonium Cations. *J. Phys. Chem. B* **2004**, *108* (33), 12271−12275.
(44) Houssin, C. J. Y.; Mojet, B.L.; Kirschhock, C.E.A.; Buschmann, V.; Jacobs, P.A.; Martens, J.A.; van Santen, R. A. 02-O-01-Small angle X-ray scattering on TPA-Silicalite-1 precursors in clear solutions: influence of silica source and cations. *Stud. Surf. Sci. Catal.* **2001**, *135*, 140.
(45) Brinker, C. J. Hydrolysis and condensation of silicates: Effects on structure. Journal of Non-Crystalline Solids. *J. Non-Cryst. Solids* **1988**, *100* (1), 31−50.
(46) Cihlář, J. Hydrolysis and polycondensation of ethyl silicates. 1. Effect of pH and catalyst on the hydrolysis and polycondensation of tetraethoxysilane (TEOS). *Colloids Surf., A* **1993**, *70* (3), 239−251.
(47) Buckley, A. M.; Greenblatt, M. The Sol-Gel Preparation of Silica Gels. *J. Chem. Educ.* **1994**, *71* (7), 599.
(48) Sefcik, J.; McCormick, A. V. Thermochemistry of aqueous silicate solution precursors to ceramics. *AIChE J.* **1997**, *43* (11), 2773−2784.
(49) Rimer, J. D.; Vlachos, D. G.; Lobo, R. F. Evolution of Self-Assembled Silica−Tetrapropylammonium Nanoparticles at Elevated Temperatures. *J. Phys. Chem. B* **2005**, *109* (26), 12762−12771.
(50) Fedeyko, J. Silica Self-Assembly in Basic Aqueous Solutions. Ph.D. Thesis, University of Delaware, 2006.
(51) Kumar, M.; Choudhary, M. K.; Rimer, J. D. Transient Modes of Zeolite Surface Growth from 3D Gel-like Islands to 2D Single Layers. *Nat. Commun.* **2018**, DOI: 10.1038/s41467-018-04296-4.
(52) Rimer, J. D.; Trofymluk, O.; Lobo, R. F.; Navrotsky, A.; Vlachos, D. G. Thermodynamics of Silica Nanoparticle Self-Assembly in Basic Solutions of Monovalent Cations. *J. Phys. Chem. C* **2008**, *112* (38), 14754−14761.
(53) Rivas-Cardona, A.; Shantz, D. F. In Situ PFG NMR of Silicalite-1 Synthesis Mixtures. *J. Phys. Chem. C* **2011**, *115* (26), 13016−13026.
(54) Rimer, J. D.; Trofymluk, O.; Navrotsky, A.; Lobo, R. F.; Vlachos, D. G. Kinetic and Thermodynamic Studies of Silica Nanoparticle Dissolution. *Chem. Mater.* **2007**, *19* (17), 4189−4197.
(55) Olafson, K. N.; Li, R.; Alamani, B. G.; Rimer, J. D. Engineering Crystal Modifiers: Bridging Classical and Nonclassical Crystallization. *Chem. Mater.* **2016**, *28* (23), 8453−8465.
(56) Ren, N.; Bosnar, S.; Bronić, J.; Dutour Sikirić, M.; Mišić, T.; Svetličić, V.; Mao, J.-J.; Antonić Jelić, T.; Hadžija, M.; Subotić, B. Role of Subcolloidal (Nanosized) Precursor Species in the Early Stage of the Crystallization of Zeolites in Heterogeneous Systems. *Langmuir* **2014**, *30* (28), 8570−8579.
(57) Sharma, P.; Yeo, J.-g.; Han, M. H.; Cho, C. H. Knobby surfaced, mesoporous, single-phase GIS-NaP1 zeolite microsphere synthesis and characterization for H2 gas adsorption. *J. Mater. Chem. A* **2013**, *1* (7), 2602−2612.
(58) Lok, B. M.; Cannan, T. R.; Messina, C. A. The role of organic molecules in molecular sieve synthesis. *Zeolites* **1983**, *3* (4), 282−291.
(59) Lowe, B. M. An equilibrium model for the crystallization of high silica zeolites. *Zeolites* **1983**, *3* (4), 300−305.
(60) Caratzoulas, S.; Vlachos, D. G.; Tsapatsis, M. Molecular Dynamics Studies on the Role of Tetramethylammonium Cations in the Stability of the Silica Octamers Si8 in Solution. *J. Phys. Chem. B* **2005**, *109* (20), 10429−10434.
(61) Oleksiak, M. D.; Rimer, J. D. Synthesis of zeolites in the absence of organic structure-directing agents: factors governing crystal selection and polymorphism. *Rev. Chem. Eng.* **2014**, *30*, 1−49.
(62) Chawla, A.; Li, R.; Jain, R.; Clark, R. J.; Sutjianto, J. G.; Palmer, J. C.; Rimer, J. D. Cooperative effects of inorganic and organic structure-directing agents in ZSM-5 crystallization. *Molecular Systems Design & Engineering* **2018**, *3* (1), 159−170.
(63) Alexander, G. B.; Heston, W. M.; Iler, R. K. The Solubility of Amorphous Silica in Water. *J. Phys. Chem.* **1954**, *58* (6), 453−455.
(64) Fleming, B. A.; Crerar, D. A. Silicic acid ionization and calculation of silica solubility at elevated temperature and pH application to geothermal fluid processing and reinjection. *Geothermics* **1982**, *11* (1), 15−29.
(65) Chan, S. H. A review on solubility and polymerization of silica. *Geothermics* **1989**, *18* (1−2), 49−56.
(66) Gunnarsson, I.; Arnórsson, S. Amorphous silica solubility and the thermodynamic properties of H4SiO4° in the range of 0°to 350°C at P(sat). *Geochim. Cosmochim. Acta* **2000**, *64* (13), 2295−2307.
(67) Niibori, Y.; Kunita, M.; Tochiyama, O.; Chida, T. Dissolution Rates of Amorphous Silica in Highly Alkaline Solution. *J. Nucl. Sci. Technol.* **2000**, *37* (4), 349−357.
(68) Oleksiak, M. D.; Soltis, J. A.; Conato, M. T.; Penn, R. L.; Rimer, J. D. Nucleation of FAU and LTA Zeolites from Heterogeneous Aluminosilicate Precursors. *Chem. Mater.* **2016**, *28* (14), 4906−4916.
(69) Busey, R. H.; Mesmer, R. E. IONIZATION EQUILIBRIA OF SILICIC-ACID AND POLYSILICATE FORMATION IN AQUEOUS SODIUM-CHLORIDE SOLUTIONS TO 300-DEGREES-C. *Inorg. Chem.* **1977**, *16* (10), 2444−2450.
(70) Shete, M.; Kumar, M.; Kim, D.; Rangnekar, N.; Xu, D.; Topuz, B.; Agrawal, K. V.; Karapetrova, E.; Stottrup, B.; Al-Thabaiti, S.; Basahel, S.; Narasimharao, K.; Rimer, J. D.; Tsapatsis, M. Nanoscale Control of Homoepitaxial Growth on a Two-Dimensional Zeolite. *Angew. Chem., Int. Ed.* **2017**, *56* (2), 535−539.
(71) Iler, R. K. Effect of adsorbed alumina on the solubility of amorphous silica in water. *J. Colloid Interface Sci.* **1973**, *43* (2), 399−408.
(72) Addai-Mensah, J.; Li, J.; Rosencrance, S.; Wilmarth, W. Solubility of Amorphous Sodium Aluminosilicate and Zeolite A Crystals in Caustic and Nitrate/Nitrite-Rich Caustic Aluminate Liquors. *J. Chem. Eng. Data* **2004**, *49* (6), 1682−1687.
(73) Ejaz, T.; Jones, A. G.; Graham, P. Solubility of Zeolite A and Its Amorphous Precursor under Synthesis Conditions. *J. Chem. Eng. Data* **1999**, *44* (3), 574−576.
(74) Prodinger, S.; Vjunov, A.; Hu, J. Z.; Fulton, J. L.; Camaioni, D. M.; Derewinski, M. A.; Lercher, J. A. Elementary Steps of Faujasite Formation Followed by in Situ Spectroscopy. *Chem. Mater.* **2018**, *30* (3), 888−897.
(75) Flory, P. J. *Principles of Polymer Chemistry*; Cornell University Press: Ithaca, NY, 1953.


DOI: 10.1021/acs.iecr.8b01695
*Ind. Eng. Chem. Res.* XXXX, XXX, XXX−XXX